Differential charge-transfer cross sections for Na^+ with Rb collisions at low energies

T. G. Lee,[1,*] H. Nguyen,[1] X. Flechard,[1,2] B. D. DePaola,[1] and C. D. Lin[1,*]
[1]*J. R. Macdonald Laboratory, Department of Physics, Kansas State University, Manhattan, Kansas 66506-2601*
[2]*LPC CAEN, Boulevard du Maréchal Juin, 14050 Caen Cedex, France*
(Received 1 April 2002; published 1 October 2002)

We report on a theoretical and experimental study of state-selective differential single-electron transfer cross sections between Na^+ ions and Rb($5s,5p$) atoms at collision energies of 2, 5, and 7 keV. A two-center multichannel semiclassical impact parameter close-coupling method with straight-line trajectories was used to obtain single-electron capture amplitudes. By combining with the eikonal approximation, we calculated the angular differential cross sections. These results are compared to the experimental data obtained with Rb targets cooled in a magnetic optical trap. It is shown that there is generally a good agreement between the present calculations and the experiments. In spite of the higher resolution offered from the cold target, the rapid oscillations in the differential cross sections are not resolved by the experiments.

DOI: 10.1103/PhysRevA.66.042701 PACS number(s): 34.10.+x, 34.70.+e, 34.50.Pi

I. INTRODUCTION

When an ion collides with an atom, processes such as excitation, charge exchange, and ionization can occur. For slow ion-atom collisions, a charge-transfer reaction is the dominant process. There is a considerable amount of experimental measurements and theoretical calculations on electron-transfer cross sections in collisions between singly charged ions with neutral atoms. In particular, collisions between singly charged alkali ions and neutral alkali atoms have been studied since the 1960s. However, most of these studies were carried out in a higher-energy region and the final states of the charge-transfer products were not determined.

Collisions between protons as well as alkali ions with Na targets have been investigated extensively by Andersen and co-workers in the 1990s [1] (*reference within*). The differential charge-transfer cross sections have been measured [2–7] and compared to close-coupling calculations based on the two-center atomic orbitals or on molecular orbitals [8–12]. Since the differential cross section is sharply forward peaked, the theoretical results had to be folded with experimental angular resolutions and some detailed structure was lost. In this paper, we report on the results from theoretical calculations and the comparison with experimental results obtained from the so-called magneto-optical trap and target recoil momentum spectrometer (MOTRIMS) apparatus at Kansas State University. The setup allows the determination of state-selective charge-transfer cross sections, as well as the differential cross section to each state. Specifically, we focus on the collisions of Na^+ ions with Rb, either initially in the $5s_{1/2}$ ground state or initially in the excited $5p_{3/2}$ states. Collision energies are 2, 5, and 7 keV in the laboratory frame. We will concentrate on the differential cross sections for capture to the dominant final states.

The rest of the paper is organized as follows. In Sec. II, the essentials of the MOTRIMS experiment are briefly discussed. The semiclassical close-coupling method and the parameters for modeling the collision as a one-electron system are described in Sec. III. The results of the calculated differential cross sections and the comparison with experimental data are given in Sec. IV. It is shown that the current experimental angular resolutions are still incapable of testing the oscillations predicted in the theory. A short summary is given in Sec. V. Atomic units are used throughout unless indicated otherwise.

II. EXPERIMENT

A simplified schematic of the experimental setup is shown in Fig. 1. Details of the apparatus will be presented elsewhere. Briefly, the setup consists of a magneto-optical trap (MOT) and a target recoil momentum spectrometer (TRIMS). The MOT consists of a system of diode lasers and accompanying optics, and a pair of anti-Helmholtz coils that are used to set up a magnetic-field gradient of approximately 5 G/cm. The spectrometer consists of a series of metal plates, appropriately biased to create two constant electric-field regions, followed by a field-free drift region, followed by a two-dimensional position-sensitive detector (PSD). Not shown in Fig. 1 is the vacuum chamber shared by the MOT and TRIMS. Because of the combination of the MOT and TRIMS techniques, this approach has been dubbed MOTRIMS [13].

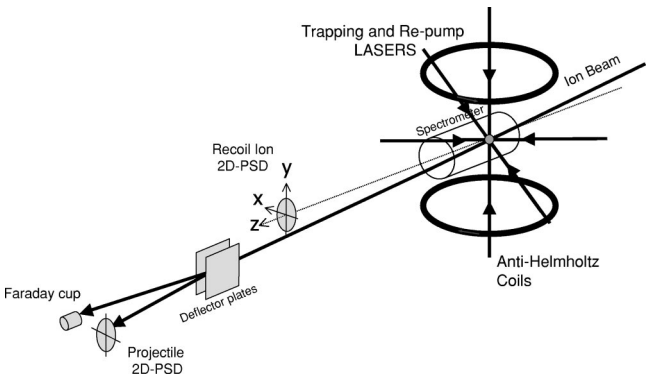

FIG. 1. Simplified schematic diagram of the experimental setup.

*Corresponding author. Email address: ltg@phys.ksu.edu/ cdlin@phys.ksu.edu

The target temperature is typically 250 μK, as determined by the ''release-and-recapture'' method. Using a measurement technique to be described below, the total target density was determined to be approximately 1×10^{10} cm^{-3}. Background pressure in the collision chamber is typically 4×10^{-9} Torr.

Excellent reviews on TRIMS exist in the literature [14–16]. Briefly, target ions created in a collision are extracted by the two sequential electric fields, and are allowed to drift in the field-free region before striking the PSD. The spectrometer geometry and electric fields are arranged so as to minimize spread in ion time of flight (TOF) and position on the PSD due to initial position. Thus, through the TOF and final position, one may deduce the recoil ion momentum vector at the time of the collision. A key concept of the TRIMS method is that one may relate the components of the recoil ion momentum to the projectile scattering angle and the collision Q value. For single-electron capture,

$$\theta_p = \frac{p_\perp}{m_p v_p} \tag{1}$$

and

$$Q = p_\parallel v_p + \frac{1}{2} v_p^2, \tag{2}$$

where θ_p is the projectile scattering angle, $p_\perp$ and $p_\parallel$ are, respectively, the recoil momenta perpendicular and parallel to the projectile axis, v_p is the projectile velocity, m_p is the projectile mass, and Q, the collision Q value, is defined by

$$Q = E_{initial}^{binding} - E_{final}^{binding}. \tag{3}$$

In general, the TOF resolution is better than the PSD resolution. Therefore, in order to optimize the resolution in Q value, the recoil spectrometer is oriented with its extraction fields nearly parallel to the projectile axis. Thus, $p_\parallel$, and therefore the Q value, is determined by time of flight.

In general, the momentum ''kick'' given to the recoil ion is comparable to the thermal momentum spread of a room-temperature atom. Thus, for the TRIMS technique to give useful momentum information, it is necessary to cool the target. Generally this is done through the precooling and supersonic expansion of the target. Here, however, the MOT provided a target that is roughly three orders of magnitude colder than available through supersonic expansion. In this system, then, the resolution is not limited by target temperature, but by other properties of the apparatus: The $p_\parallel$ is currently limited to 0.03 a.u. by the energy spread in the projectile ion beam [17]; while $p_\perp$ is limited to 0.086 a.u. by the PSD.

In this work we report on charge transfer from both the ground and first excited states of Rb. Though the trapping and cooling process leaves some fraction of the Rb in the $5p_{3/2}$ state, it is critical to determine what this fraction is. To do this we employ a different method, described in more detail elsewhere [18], which relies on both the extremely low target temperature and the tremendous Q-value resolution inherent in the MOTRIMS technique. Briefly, the trapping laser beams are chopped with a 75% duty cycle at 50 kHz. ''Laser-on'' and ''laser-off'' Q-value spectra are then compared. Because the atoms do not move an appreciable distance during a single on-off period, the change in Rb($5s$) population is exactly equal and opposite to the change in the Rb($5p$) population. One can easily show that this allows the determination of both the ratio of the $5s$ and $5p$ populations and the ratio of capture cross sections from these states. Once the excited-state fraction has been thus measured, an accurate measurement of the target fluorescence and spatial dimension is sufficient to determine the target density. Typically, excited-state fractions of 22% were obtained. Because the day-to-day excited-state fraction could vary [19], they were measured *in situ* for each cross-section measurement presented here.

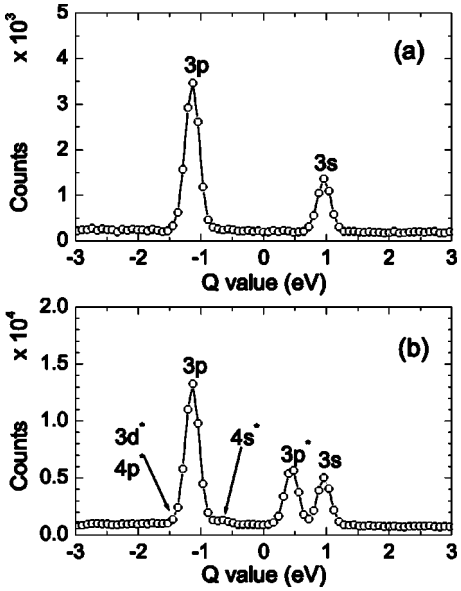

FIG. 2. Relative capture cross section versus Q value for a collision energy of 7 keV. In (a), the trapping lasers are blocked, while in (b) they are unblocked. The different channels are labeled by the final state in sodium. Asterisks indicate channels in which capture is from Rb($5p$).

Figure 2 shows an example of experimental charge-transfer cross section versus Q value, for a collision energy of 7 keV. The individual capture channels are clearly resolved. Figure 2(a) was taken when the lasers were blocked, while Fig. 2(b) was taken with the lasers unblocked. Thus, the former represents capture from the ground state only, while the latter represents capture from both ground and excited states. In comparing these two plots, the additional channels opened up through capture from Rb($5p$) are readily visible. With knowledge of the excited-state fraction, these two curves yield relative cross sections for capture, from a pure ground state and a pure excited state, into all the various final states.

In order to obtain cross-section differential in capture channel, a software gate is set on a single peak in the Q-value plot, and the corresponding PSD data are recorded. The result is integrated about the axis parallel to the beam

TABLE I. Bound-state energies of Na obtained from the model potential and the comparison with experimental data [23]. Even-tempered basis functions are used to diagonalize the atomic Hamiltonian. Energies are in atomic units.

State	Theory	Experiment
$3s$	−0.18852	−0.18886
$4s$	−0.07185	−0.07158
$5s$	−0.03748	−0.03758
$6s$	−0.01849	−0.02313
$7s$	0.09104	−0.01566
$8s$	0.53203	−0.01131
$9s$	2.41623	−0.00854
$3p$	−0.11145	−0.11154
$4p$	−0.05098	−0.05094
$5p$	−0.02902	−0.02920
$6p$	−0.00719	−0.01892
$7p$	0.10224	−0.01325
$8p$	0.70719	−0.00980
$9p$	2.19506	
$3d$	−0.05563	−0.05594
$4d$	−0.03126	−0.03144
$5d$	−0.01984	−0.02011
$6d$	0.00892	

direction; the radial position on the detector is then related to scattering cross section via Eq. (1).

III. THEORETICAL METHOD

The semiclassical close-coupling theory of atomic collisions has been described by Fritsch and Lin [20] and by Bransden and McDowell [21]. For the scattering calculation we used the same form of theory as Kuang and Lin [22]. Briefly, the time-dependent wave function is expanded in terms of bound atomic orbitals plus continuum states on each center, each with appropriate plane-wave translational factors. The atomic orbitals are expressed in terms of even-tempered basis functions

$$\phi_{nlm}=\sum_k C_{nk}N_l(\xi_k)e^{-\xi_k r}\tilde{Y}_{lm}(r), \tag{4}$$

where $\tilde{Y}_{lm}(r)$ consists of a spherical harmonic multiplied by r^l; $N_l(\xi_k)$ is a normalization constant, and the orbital exponents ξ_k are taken to form a geometric sequence

$$\xi_k=\alpha\beta^k \quad (k=1,2,\ldots,N). \tag{5}$$

Two parameters α and β can be determined by energy minimization. For low-energy alkali ion-atom collision, only the outer electron is active in the charge-transfer process. The Rb and Na are each treated as a one-electron system with the core being frozen. The active electron in each atom is governed by a model potential:

$$V_{Na}(r)=-\frac{1}{r}[1+(10+17.9635r)e^{-3.5927r}], \tag{6}$$

TABLE II. Same as in Table I, except for atomic Rb.

State	Theory	Experiment
$5s$	−0.15071	−0.15351
$6s$	−0.06215	−0.06177
$7s$	−0.03320	−0.03362
$8s$	−0.01959	−0.02116
$9s$	−0.01227	−0.01454
$10s$	−0.00828	−0.01061
$11s$	−0.00530	−0.00808
$12s$	−0.00306	
$13s$	−0.00162	
$14s$	0.30795	
$15s$	1.81277	
$5p$	−0.10272	−0.09541
$6p$	−0.04800	−0.04520
$7p$	−0.02770	−0.02657
$8p$	−0.01713	−0.01752
$9p$	−0.01024	−0.01242
$10p$	−0.00579	
$11p$	−0.00305	
$12p$	0.04485	
$13p$	0.66372	
$5d$	−0.03360	−0.03640
$6d$	−0.02111	−0.02279

$$V_{Rb}(r)=-\frac{1}{r}[1+(36-1.975r)e^{-2.34113r}]. \tag{7}$$

The parameters in these model potentials are chosen such that the experimental binding energies of the first few states of interest are well reproduced. In fitting the potential parameters, the wave functions are calculated numerically. Once the potential is chosen, we then make sure that the atomic orbitals are adequately represented by combinations of even-tempered functions, with properly adjusted α and β parameters.

In the present close-coupling calculations with atomic orbitals on the two collision centers, we have a set of 33 atomic states with $l\leqslant 2$ in the Na center. Similarly, a set of 35 atomic states with $l\leqslant 2$ is used for the Rb target. In order to assure the size of the basis set used is adequate for converged results, we have checked the state-selective capture probabilities with a larger basis set (i.e., $l\leqslant 3$) for a few impact parameters and found that the difference between the two sets calculation is about 1–3 %, and thus this will not significantly alter the results of our calculations.

Tables I and II show the energies of the bound and pseudocontinuum states of Na and Rb, respectively, used in the close-coupling calculation. For the bound states, the binding energies obtained from the model potentials are also compared to the experimental values [23]. The pseudostates are used in the basis set to help describing the distortion of the electronic orbitals at smaller internuclear separations. For the three collision energies dealt with here, the charge-

transfer amplitudes oscillate rapidly with impact parameters. To ensure good convergence in the differential and total charge-transfer cross sections, we calculated up to 203 impact parameters. For each impact parameter, the coupled equations from the close-coupling approximation are integrated from $\nu t = -200$ to $+250$ a.u. We consider collisions with Rb initially in the ground state, as well as in the $5p$ state.

To obtain the differential cross sections, we employ the eikonal approximation [21]. The angle-differential cross section (DCS) for an inelastic transition from an initial state i to a final state f can be written as the absolute square of a scattering amplitude A_{fi} at a given angle θ,

$$\frac{d\sigma_{fi}}{d\theta} = 2\pi \sin\theta |A_{fi}|^2, \tag{8}$$

where the scattering amplitudes A_{fi} are determined in turn from the impact-parameter-dependent transition amplitudes, and are given by

$$A_{fi}(\theta) = \gamma \int_0^{+\infty} bF(b)dbJ_{|m_f - m_i|}\left(2b\mu\nu \sin\frac{\theta}{2}\right). \tag{9}$$

Here

$$F(b) = C_{fi}(b, +\infty)e^{2(i/\nu)Z_T Z_P \ln b}, \tag{10}$$

with $\gamma = \mu\nu(-i)^{|m_f - m_i|+1}$, μ the reduced mass, ν the relative collision velocity, and m_f (m_i) the magnetic quantum number of the final (initial) state. The function J denotes a Bessel function of the first kind and C_{fi} is the semiclassical transition amplitude, evaluated for a given impact parameter b. The additional phase $e^{2(i/\nu)Z_T Z_P \ln b}$ is the eikonal phase due to the Coulomb repulsion between the two nuclei and Z_T (Z_P) is the effective charge of the target (projectile) that defines the Coulomb trajectory of the two colliding nuclei. Since charge-transfer occurs far outside the core of both atomic ions, an effective charge of 1 was used for each.

The numerical evaluation of the diffraction integral (9) should be done carefully since it involves rapidly oscillating integrands. We divide the range of impact parameters into small sectors, and within each sector the integrand is expressed as $F(b)\exp(i\omega \ln b)$. The evaluation of the integral over the sector is done by substituting $x = \ln b$ and rewriting the integral to be in the form of

$$\int_{x_n}^{x_{n+1}} (ax^2 + bx + c)\exp(iwx)dx, \tag{11}$$

where we have fitted the function $F(b)$ within the sector by a quadratic function. The integration over this sector can then be performed analytically. For a converged result, it is essential to ensure that within each sector the function $F(b)$ is well behaved with respect to $x = \ln b$. The accuracy of this algorithm can be checked by varying the size of the sectors or by using another algorithm, such as the Simpson rule. We further check that the total cross sections obtained by integrating DCS over scattering angles and by integrating electron-capture probabilities over impact parameters are identical.

IV. RESULTS AND DISCUSSION

In this section, we present the calculated differential cross sections for various final states and compare these to the experimental measurements by folding the calculated cross sections with the experimental angular resolution. We also provide impact-parameter weighted probabilities and the unconvoluted DCS to show that the current experimental resolution is insufficient to confirm the predicted oscillatory structures. Both scattering angles and differential cross sections are referenced to the laboratory frame.

A. $Na^+ + Rb(5s)$

For collision energies of 2, 5, and 7 keV, the two dominant charge-transfer channels in $Na^+ + Rb(5s)$ collisions are into $Na(3s)$ and $Na(3p)$ states. The total charge-transfer cross section for each state was obtained from

$$\sigma_{nl} = 2\pi \sum_m \int_0^{+\infty} bdb|C_{fi}(b, +\infty)|^2. \tag{12}$$

From Table III, we see that in this energy range, capture to $3p$ dominates over $3s$. All the other channels are much weaker and are not observed in the experiment except at the highest collision energy where capture to $Na(3d)$ represents only a few percent of the total measured cross section. The fact that these are the two dominant channels can be understood from the degree of inelasticity for each transition. In Fig. 3, the energy levels of the collision system are shown. For $Rb(5s) \rightarrow Na(3s)$, the transition is exoergic process with a Q value of $+0.0354$ a.u., whereas for $Rb(5s) \rightarrow Na(3p)$, the process is endoergic, with $Q = -0.0419$ a.u. From the asymptotic energy levels, it would appear that the dominant transition would be to the $Na(3s)$ state, which not what is observed either experimentally or from the theoretical calculations.

A proper framework to understand the calculated results is best if based on the molecular potential curves. In the atomic orbitals close coupling (AOCC) approach, such curves are not calculated. Based on the model potentials (6) and (7), we have calculated the adiabatic potential curves of $NaRb^+$, and the results are shown in Fig. 4. These curves are very similar

TABLE III. Theoretical integral cross sections (10^{-16} cm^2) for charge transfer from ground-state $Rb(5s)$ to final states. The third line shows the comparison between theory and experiment of the capture cross-section ratio $Na(3s)/Na(3p)$.

Final state	$E = 2$ keV	$E = 5$ keV	$E = 7$ keV
$Na(3s)$	1.06	6.02	8.41
$Na(3p)$	19.16	20.59	22.35
Theory	0.055	0.292	0.376
MOTRIMS	0.020 ± 0.005	0.250 ± 0.032	0.271 ± 0.015

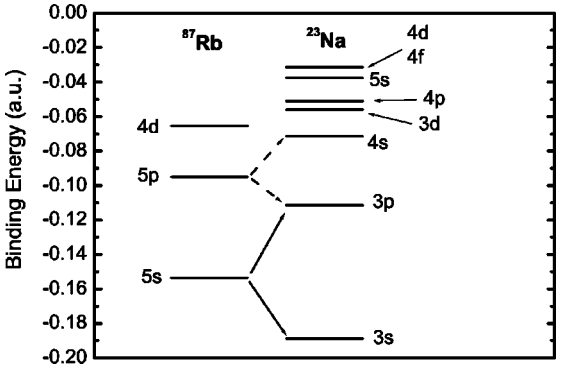

FIG. 3. Energy levels of ^{87}Rb and ^{23}Na atoms.

to those calculated by Melius and Goddard [8] for the $Li^+ + Na$ system. From these curves, it is clear that transition to Na($3s$) from Rb($5s$) is dictated by the radial coupling between the two Σ states, which show an avoided crossing near $R=13$ a.u. For the transition to Na($3p$), there are two possibilities. A radial coupling between two Σ curves would populate the $3p_0$ final state, while a rotational coupling between Σ and Π states would populate the $3p_1$ final state. For the latter, the two curves cross near $R=6$ a.u., and this crossing is an efficient mechanism for populating the Na($3p$) state at low energies. In fact, the calculated electron-capture probability [see Fig. 7(b)] for the $3p_1$ substate does indeed peak near 6.0 a.u.

We now examine the differential cross sections for these two dominant channels; see Fig. 5. In order to compare with the MOTRIMS measurements, we performed a Gaussian convolution on the theoretical results with an angular resolution of 73.64, 87.2, and 138.0 μrad for 7, 5 and 2 keV, respectively. The experimental results are normalized to the theoretical predictions at the peak for easy comparison.

From Fig. 5(b), it is clear that there is an excellent agreement between theory and experiment for the dominant Rb($5s$)$\rightarrow$Na($3p$) channel. For the weaker Na($3s$) channel, the agreement is quite good at 7 keV, but significant deviations can be seen at 2 keV. At this energy, the total cross section to $3s$ is only about 5% of the capture to $3p$. The smaller cross section is reflected in the larger errors in the theoretical DCS, and the increased experimental uncertainty that is dominated by counting statistics.

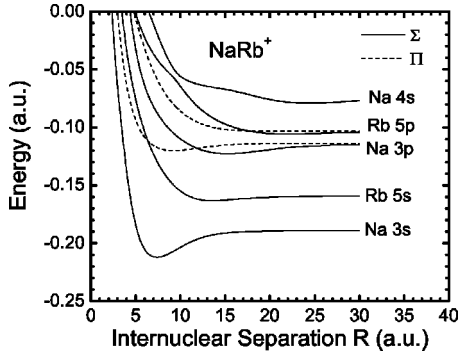

FIG. 4. Adiabatic potential curves for the $NaRb^+$ molecule.

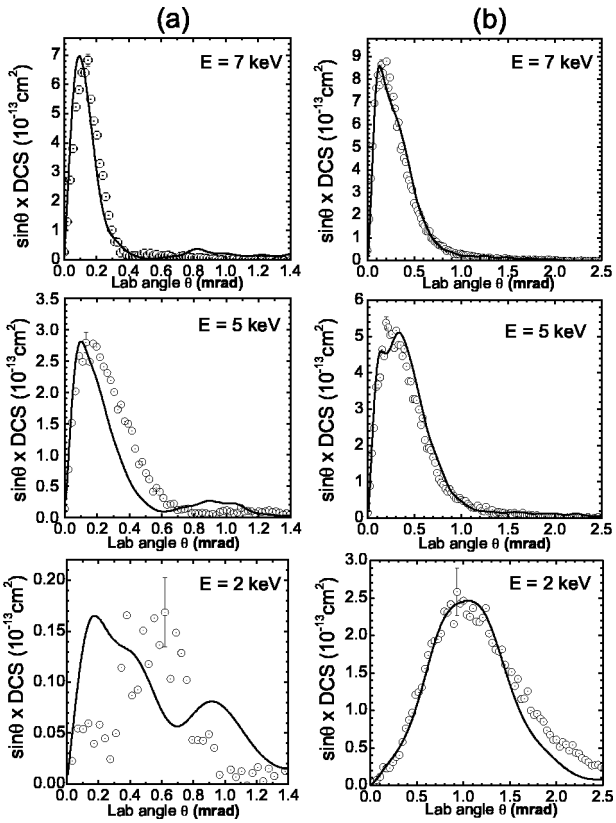

FIG. 5. (a) $\sin\theta\times$DCS as functions of laboratory scattering angle θ for Rb($5s$)-Na($3s$) at impact energies from 7 to 2 keV. The $\odot$ represents the MOTRIMS data and solid line denotes theoretical calculations folded with experimental angular resolution. The experimental results have been normalized to the theoretical data. (b) is the same as (a), except for Rb($5s$)$\rightarrow$Na($3p$) channel. Note the difference in the angular scale.

Another observation is that the DCS for capture to $3s$ is peaked at smaller angles, reflecting the fact that capture occurs at larger impact parameters. In contrast, capture to $3p$ occurs at larger scattering angles, reflecting the efficient rotational coupling at internuclear distance at about 6 a.u.

The DCS in Fig. 5 for different energies can be put on the same graph if we plot the DCS against $E\theta$. This is done in Fig. 6(a) for the experimental data for capture to the dominant $3p$ channel. In Fig. 6(b), the same data from the theoretical calculations without convolution are presented. It is clearly seen that the predicted DCS show many oscillations with respect to the scattering angle. Such oscillations are expected for collisions at low energies. Unfortunately, limitations in the angular resolution of the current MOTRIMS apparatus make the observation of such oscillations impossible.

In Fig. 7, we illustrate the interplay between the calculated impact-parameter-dependent electron-capture probabilities and the differential cross sections for the Rb($5s$)-Na($3p$) transition. We also show the dependence on the magnetic quantum number. The dominant contribution

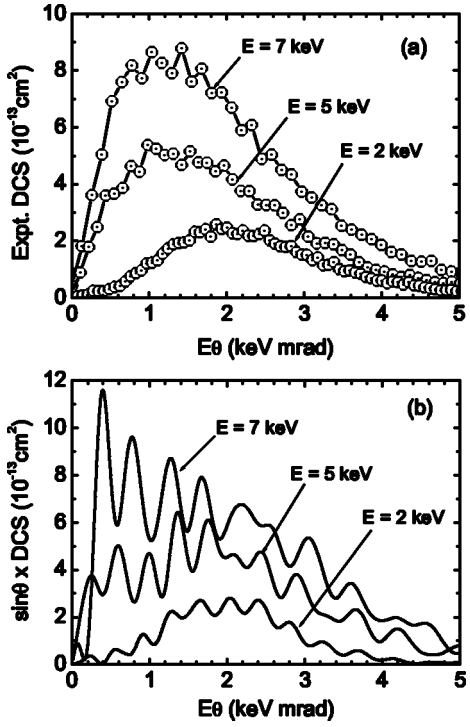

FIG. 6. (a) Experimental DCS as functions of scaled laboratory scattering angle $E\theta$ for Rb($5s$)-Na($3p$) at impact energies from 7 to 2 keV. Experimental data are normalized to the TCAOCC calculations. (b) is the same as (a) except that these are the results from TCAOCC calculations.

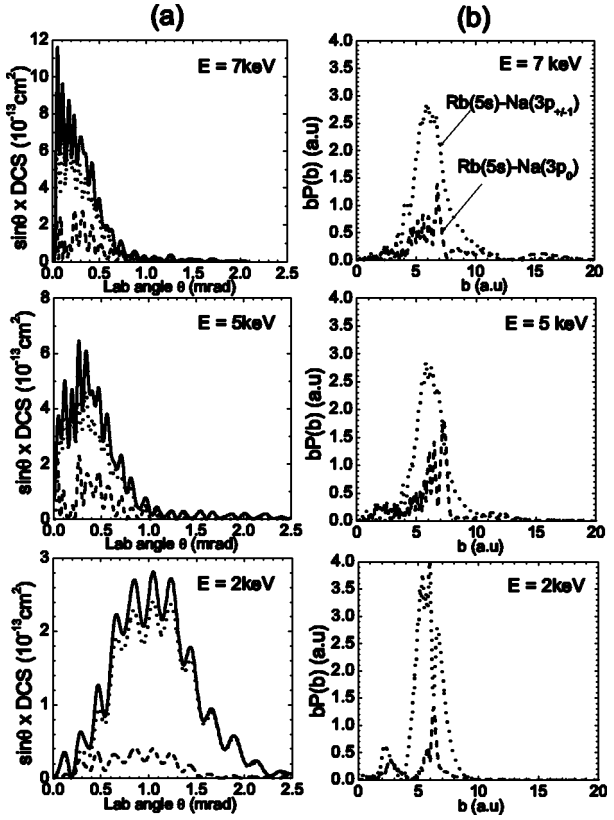

FIG. 7. (a) Theoretical sin θ-weighted DCS as functions of scattering angle θ of charge transfer for Rb($5s$)$\rightarrow$Na($3p$) for impact energies of 7–2 keV. The dotted line and dashed line denotes capture to Na($3p_{\pm 1}$) and Na($3p_0$), respectively. The solid line represents the total DCS. (b) The corresponding impact-parameter b-weighted probabilities as functions of b.

from the rotational coupling near $R=6$ a.u. is quite clear from the impact-parameter-dependent probabilities, but not as clear from the differential cross sections.

B. $Na^+ + Rb(5p)$

For collisions of Na^+ with the excited Rb($5p$) states at energies of 2, 5, and 7 keV, the dominant processes are electron capture to the $3p$ and $4s$ states. This can be anticipated from the energy-level diagram, Fig. 3, as well as from the potential curves in Fig. 4. The calculated total cross sections are listed in Table IV. In these calculations, the initial $5p$ state is assumed to be randomly oriented, and the magnetic substates are distributed statistically, since the lasers are incident from three orthogonal directions. The total cross section for the dominant $3p$ channel is very large, reflecting electron capture occurring at large impact parameters. For the weaker channel, i.e., electron capture to the $4s$ state, the calculated total cross section has a minimum at 5 keV. In Table IV, we also present the cross-section ratio for $4s$ with respect to $3p$, and compare the results with the experimental measurement. The agreement is quite good except at 5 keV, where the calculated result is outside the measured uncertainty.

First we anticipate the mechanism for the capture of a Rb($5p$) electron to Na($3p$) and Na($4s$) in terms of the potential curves of Fig. 4. Radial coupling will take an initial Rb($5p_0$) to Na($3p_0$), and the rotational coupling will take it to Na($3p_1$). The rotational coupling is weak since there is no curve crossing. Thus the radial coupling, which has a slightly avoided crossing at large R near 22 a.u., is expected to be the dominant one. Similarly, if the initial state is Rb($5p_1$), the radial coupling will take it to Na($3p_1$), and the rotational coupling will take it to Na($3p_0$). Again, the radial coupling is expected to dominate, and there is a weak avoided crossing between the two Π curves at R near 15 a.u. We thus expect transition to Na($3p$) to be quite large and to occur at large impact parameters. For transition to Na($4s$), the energy gap at large R is more, thus transitions at larger impact parameters would be smaller, especially when the collision energy is decreased. At the lower energies, the avoided crossing

TABLE IV. Theoretical integral cross sections (10^{-16} cm^2) for charge transfer from Rb($5p$) to final states. The third line shows the comparison between theory and experiment of the capture cross-section ratio Na($4s$)/Na($3p$)

Final state	$E=2$ keV	$E=5$ keV	$E=7$ keV
Na($4s$)	10.39	5.03	8.92
Na($3p$)	94.20	132.82	129.10
Theory	0.110	0.038	0.069
MOTRIMS	0.128 ± 0.053	0.072 ± 0.009	0.080 ± 0.011

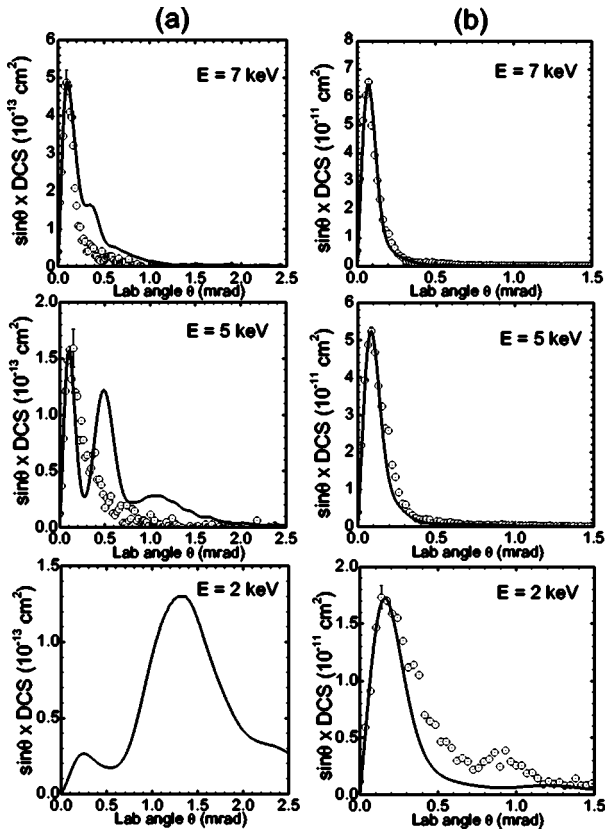

FIG. 8. (a) Same as Fig. 5 but for charge-transfer from Rb($5p$) to Na($4s$). Solid line denotes the TCAOCC and ⊙ represents the experimental data. (b) is the same as (a), except for Rb($5p$) →Na($3p$) channel.

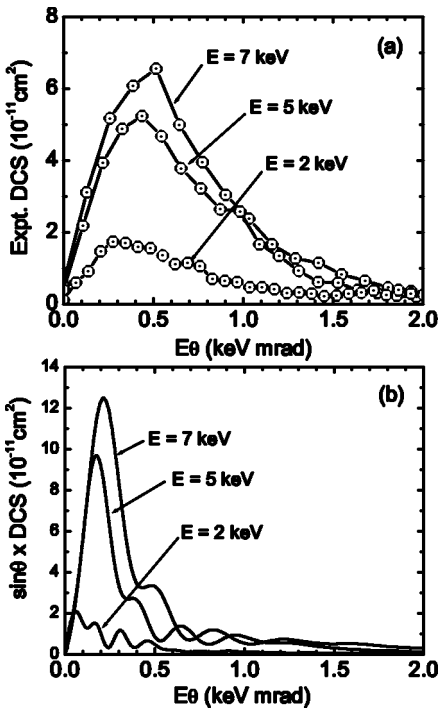

FIG. 9. Same as Fig. 6 but for charge transfer from Rb($5p$) to Rb($3p$).

between the two Σ curves at R near 9 a.u. should be more efficient in populating the Na($4s$) state. In the following, we show that this qualitative interpretation is consistent with the calculated electron-capture probabilities.

In Fig. 8, the theoretical differential cross sections, after they have been convoluted with the experimental resolution, are compared to the measured cross sections. For Rb($5p$) →Na($3p$), the theoretical DCS agrees perfectly with the experimental measurement at 7 keV. At 5 keV, there is only a minor discrepancy. At 2 keV, the experimental DCS at larger angles is greater than what theory predicts. For the weak channel [i.e., Rb($5p$)→Na($4s$)], the overall agreement is less satisfactory. At 7 keV, the agreement at small angles is quite good, but the theory shows a shoulder at the higher energies. At 5 keV, the agreement between theory and experiment is only fair, and it appears that the shoulder at 7 keV becomes a pronounced peak at 5 keV. At 2 keV, the experimental signal is too weak to extract useful information, but the shoulder from theory at 7 keV appears to the major peak. We interpret this structure as being due to the avoided crossing of the two Σ curves. At 7 keV, the transition is dominated by the coupling at large R, thus the DCS is rather forward peaked. As the energy is decreased, the system evolves more adiabatically and probabilities for transitions at large R decrease. At 2 keV, transitions at large R become insignificant, and the major mechanism for transition occurs at the avoided crossing near $R=9$ a.u. The calculated electron-capture probabilities to Na($4s$) (not shown) indeed demonstrate this behavior, which can also be seen from the theoretical differential cross sections in Fig. 8(a). The mechanism also explains the minimum of the total cross section to Na($4s$) at 5 keV. Above this energy, transitions occur mostly at large impact parameters. Below this energy, the Landau-Zener-type transition near $R=9$ a.u. becomes more efficient such that the cross section increases with decreasing collision velocity. This interpretation is consistent with the calculated total cross sections and the differential cross sections.

In Fig. 9 we compare the DCS versus $E\theta$ for the three collision energies for the Rb($5p$)-Na($4p$) transition. On the top frame the experimental results are shown. On the bottom frame, the theoretical results without the convolution with angular resolution are shown. Apparently, the calculated angular distributions are peaked much more in the forward angles than the experimental measurements. Until the experimental angular resolution is improved to the point of being able to resolve the predicted rapid oscillations in DCS, the predicted propensity for forward peaking cannot be stringently tested.

V. SUMMARY

In summary, we have used the combination of two-center atomic-orbital close-coupling method and eikonal approximation to perform a detailed calculation on the charge-transfer differential cross section of Na^+-Rb collision at im-

pact energies of 2, 5, and 7 keV. We have shown that the theoretical results agree extremely well with experiments for the dominant charge-transfer channels. However, for the weak channels, the agreement is less satisfactory. This discrepancy may indicate a sign of failure both in theory and experiment, in obtaining accurate results for the weak channels. We have also shown that the present MOTRIMS results are still unable to test the oscillatory structures predicted for the DCS, in particular, for transitions from excited initial states. However, an improvement of the experimental resolution is in progress, and it is hoped that a more precise measurement will display these oscillations.

ACKNOWLEDGMENTS

This work was supported by the Chemical Sciences, Geosciences and Biosciences Division, Office of Basic Energy Sciences, Office of Science, the U.S. Department of Energy. T.G.L. wishes to thank Dr. Brett Esry for providing the code to calculate the MO potential curves.

[1] D. Dowek, I. Reiser, S. Grego, N. Andersen, A. Dubois, J.C. Houver, S.E. Nielsen, C. Richter, J. Salgado, A. Svensson, and J.W. Thomsen, J. Phys. B **35**, 705 (2002).
[2] J. Perel, R.H. Vernon, and H.L. Daley, Phys. Rev. **138**, A937 (1965).
[3] V. Aquilanti and G. Bellu, J. Chem. Phys. **61**, 1618 (1974).
[4] F. von Busch, J. Hormes, and H. Liesen, Chem. Phys. Lett. **34**, 244 (1975).
[5] R.W.V. Resandt, C. de Vreugd, R. Champion, and J. Los, Chem. Phys. **29**, 151 (1978).
[6] T. Okamoto, Y. Sato, N. Shimakura, and H. Inouye, J. Phys. B **14**, 2379 (1981).
[7] M. van der Poel, C.V. Nielsen, M.A. Gearba, and N. Andersen, Phys. Rev. Lett. **87**, 123201 (2001).
[8] C.F. Melius and W.A. Goddard, Jr., Phys. Rev. A **10**, 1541 (1974).
[9] A. Dubious, S.E. Nielsen, and J.P. Hansen, J. Phys. B **26**, 705 (1993).
[10] S. Nielsen, J.P. Hansen, and A. Dubious, J. Phys. B **28**, 5295 (1993).
[11] M. Machholm, E. Lewartowski, and C. Courbin, J. Phys. B **27**, 4681 (1994).
[12] M. Machholm and C. Courbin, J. Phys. B **29**, 1079 (1996).
[13] X. Flechard, H. Nguyen, E. Wells, I. Ben-Itzhak, and B.D. DePaola, Phys. Rev. Lett. **87**, 123203 (2001).
[14] J. Ullrich, R. Moshammer, R. Dörner, O. Jagutzki, V. Mergel, H. Schmidt-Böcking, and L. Spielberger, J. Phys. B **30**, 2917 (1997).
[15] R. Dörner, V. Mergel, O. Jagutzki, L. Spielberger, J. Ullrich, R. Moshammer, and H. Schmidt-Böcking, Phys. Rep. **330**, 95 (2000).
[16] R. Moshammer, M. Unverzagt, W. Schmitt, J. Ullrich, and H. Schmidt-Böcking, Nucl. Instrum. Methods Phys. Res. B **108**, 425 (1996).
[17] An ion-beam energy spread of 1 eV out of 6 keV is sufficient to limit the *Q*-value resolution to the observed value.
[18] X. Flechard, H. Nguyen, S.R. Lundeen, M. Stauffer, H.A. Camp, C.W. Fehrenbach, and B.D. DePaola, Phys. Rev. Lett. (to be published).
[19] The excited-state fraction in a MOT has until now, not been easy to characterize. It is known, however, to depend on the detuning and power of the trapping laser, as well as on the alignment of the six laser beams comprising the MOT. Clear characterization of the excited-state fraction in a MOT will be the subject of future work.
[20] W. Fritsch and C.D. Lin, Phys. Rep. **202**, 1 (1991).
[21] B.H. Bransden and M.R.C. McDowell, *Charge Exchange and Theory of Ion-Atom Collisions*, The International Series of Monographs on Physics Vol. 82 (Clarendon, Oxford, 1992).
[22] Jiyun Kuang and C.D. Lin, J. Phys. B **29**, 1207 (1996).
[23] C.E. Moore, *Atomic Energy Levels* (National Bureau of Standards, Washington, D.C., 1971), Vols. I and II.